Alternative Feedstock and Spatial Sampling Variability for Enhanced Mineral Weathering in Agricultural Settings

Madeline F. Bartels
Advisor: Noah Planavsky
Second Reader: Michael Oristaglio
December 13th, 2023

A senior thesis presented to the Department of Earth and Planetary Sciences, Yale University, in partial fulfillment of the Bachelor's degree.

In presenting this essay in partial fulfillment of the Bachelor's Degree from the Department of Earth and Planetary Sciences, Yale University, I agree that the department may make copies or post it on the departmental website so that others may better understand the undergraduate research of the department. I further agree that extensive copying of this thesis is allowable only for scholarly purposes. It is understood, however, that any copying or publication of this thesis for commercial purposes or financial gain is not allowed without my written consent.

Madeline Bartels, December 13th, 2023

Alternative Feedstock and Spatial Sampling Variability for Enhanced Mineral Weathering in Agricultural Settings

Madeline F. Bartels

ABSTRACT

There is a critical need to develop precise monitoring, reporting, and verification (MRV) practices for carbon removal strategies such as enhanced mineral weathering (EMW). To help address current gaps in knowledge, basalt and steel slag were applied to corn-soybean rotation plots at Carleton College in Minnesota as part of an ongoing EMW trial. The concentrations of mobile (Na, Mg, Ca) and immobile (Ti, Th) elements changed heterogeneously in the control, basalt-amended, and slag-amended plots. When the TiCAT framework method was used to compare mobile and immobile elemental concentrations from pre- and post-feedstock amendment soil samples, elemental values fell outside of the anticipated range and carbon dioxide removal (CDR) rates could not be accurately calculated. This investigation concludes that baseline soil samples were not collected at a great enough spatial granularity, leading to irregularities in collected data.

The second part of this study evaluates the number of soil samples required to capture natural spatial soil elemental variation. A statistical simulation comparing the number of samples averaged to the deviation from the true sample set mean was run on soil sample sets from Haliburton Forest in Ontario and Carleton College in Minnesota. This analysis concluded that the sampling practices used to collect both sample sets insufficiently captured spatial variation in baseline soils. Simulation results suggest that the original Minnesota EMW sample set size of 12 soil samples should be increased to 30 soil samples during both baseline and post-feedstock amendment sampling. By increasing confidence in soil elemental values, researchers can more accurately constrain CDR rates to develop clear MRV approaches, supporting the global scaling of EMW projects.

INTRODUCTION

The rapid upscaling of carbon dioxide removal (CDR) research and implementation is a critical strategy for mitigating the damages caused by anthropogenic climate change. The world currently emits 40 Gt CO_2 per year (IPCC, 2018), a quantity far surpassing the drawdown capacity of natural biologic, geologic, and oceanic sinks, leading to an accumulation of CO_2 and other greenhouse gasses (GHGs) in the atmosphere (Chilingar et al., 2009). 45 Mt of CO_2 is captured annually by negative emission technology facilities (IEA, 2022), but in order to limit global warming to 2 ºC, a yearly average of 9 Gt must be captured until the end of the twenty-first century (Beerling et al., 2020; Smith et al., 2023). After 2100, this annual drawdown requirement increases to 20 Gt (UNEP, 2017; National Academies of Sciences Engineering and Medicine, 2019). It is evident that a combination of natural and technological CDR methods are required to attain the climate goals outlined in the Paris Agreement (UNFCCC, 2015; Smith et al., 2023).

One scalable and effective method of carbon capture is enhanced mineral weathering (EMW). This method aims to increase the global rate of silicate weathering by applying crushed rocks to agricultural fields, coastlines, forests, and marginal lands. Mafic-ultramafic minerals are the primary sites of silicate weathering, which progresses according to the simplified reaction:

$$CaSiO_3 + H_2O + 2CO_2 \rightarrow CaCO_3 + SiO_2 + H_2O + CO_2$$

In practice, rocks applied to EMW sites are weathered into intermediate dissolved cations (Ca^{2+}) and dissolved alkalinity (HCO_3^-). This dissolved alkalinity reaches the ocean via transport by groundwater and riverine systems and combines with cations, forming stable carbonate minerals.

Basalt is a favorable feedstock for EMW due to its widespread distribution and high content of olivine, a mineral with fast weathering kinetics (Kelemen et al., 2019). Though other minerals such as brucite and wollastonite weather faster than olivine and other silicates (Kelemen et al., 2019), their low global availability makes them poor choices of feedstock. Olivine-group silicates, on the other hand, are widely distributed across mafic and ultramafic igneous rocks at the Earth's surface. They are also common components of steel slag (Piatak et al., 2015). As development progresses and the human population grows, the global quantity of silicate waste, a byproduct of steel manufacturing, will increase. To support the re-use of this waste product, recent studies have explored the possibility of using silicate-rich steel slag and iron slag as feedstocks for ERW in agricultural settings (Renforth et al., 2011; Beerling et al., 2020; Chukwuma et al., 2021; Knapp et al., 2023). Utilizing waste streams such as alkaline mine tailings and industrial slag for EMW also advances the establishment of circular economies.

Agricultural land makes for ideal EMW testing and deployment sites. Agricultural land in the United States makes up roughly 40% of land area (USDA, 2022), and with a potential 4.9 Gt CO_2 global annual EMW storage capacity with basalt, represents a potential 0.95 Gt of CO_2 storage (USGS, 2015; Strefler et al., 2018). In addition, EMW on croplands can produce desirable co-benefits including increased crop yield due to key nutrient influx from EMW feedstocks (Guo et al., 2023; Kantola et al., 2023). Farmers are accustomed with soil sampling processes and the infrastructure for mineral spreading on cropland is already in place, since farmers commonly spread lime on their fields to increase soil pH. Switching out lime for basalt or slag feedstocks not only captures CO_2 via silicate weathering, but also introduces the additional climate benefit of reducing possible N_2O emissions from liming (Nadeem et al., 2020).

However, despite the desirable impacts of increased crop yield and other EMW co-benefits, moving to deploy EMW on agricultural lands at scale is challenging because it is difficult to constrain carbon fluxes in natural environments and accurately calculate CDR rates. A monitoring, reporting, and verification (MRV) scheme based on tightly constrained carbon flux monitoring must be developed before EMW projects can deploy at scale. There are several proposed methods for conducting EMW MRV. Electrical conductivity can be measured in soil pore water and then correlated to alkalinity, predominantly in the form of HCO_3^-, to determine the amount of carbon captured. Carbon captured as organic carbon can be measured in crop biomass, roots, and soil (Amann and Hartmann, 2022). Organic and inorganic carbon in soil samples and dissolved organic and dissolved inorganic carbon in soil pore water can be measured and compared to baseline values. These data can also be coupled to carbon isotopic signatures and soil microbial abundance to better constrain the mechanisms of CO_2 drawdown. Soil CO_2, CH_4, and N_2O emissions can be measured directly from flux chambers or towers placed at the field site (Almaraz et al., 2022).

The TiCAT framework is a recently developed EMW MRV method and is the analytical method of choice in this study (Reershemius et al., 2023). The TiCAT framework calculates CDR rates by comparing immobile Ti to mobile cations in soil samples before and after EMW application. It is assumed that Ti leaches into soil from the feedstock (basalt, slag, wollastonite) and remains immobile. This creates a stable baseline between sampling years which can be used to compare against other elements. Mobile cations, unlike Ti, weather during reactions with atmospheric CO_2 and are carried away from the sampling site. Therefore, the percentage of cation loss compared with a constant Ti value, assuming homogeneous mixing between feedstock and soil, can be used to calculate CDR rates.

Another necessary component of MRV is determining an acceptable value of baseline spatial heterogeneity and creating sampling regimes to stay under this value limit. If variation in soil detrital elements is high, achieving a clear signal during MRV measurements becomes impossible. Therefore, it is necessary to ensure that baseline soil samples are homogeneous enough to extrapolate data from sample locations to whole fields. The number of samples taken from an EMW field site must increase in proportion to the spatial variability of soil composition. This study aims to determine an appropriate spatial sampling pattern which allows for precise CDR rate calculations while minimizing the unnecessary costs, time, and physical burden of unnecessary soil sampling.

This study applies the TiCAT MRV method and spatial heterogeneity analysis to two EMW project sites: croplands in Minnesota, USA treated with basalt and steel slag and Haliburton Forest in Ontario, Canada treated with wollastonite. Our laboratory analysis methods described in the next section help us achieve a more constrained and accurate MRV approach. By working to develop an MRV scheme for an agroforestry EMW scenario, we hope to enable the widespread deployment of EMW in the USA and beyond in order to achieve global climate goals.

METHODS

Minnesota Soil Sample Collection

Twelve agricultural corn-soybean rotation plots located on the Rec Farm Field at Carleton College in Minnesota have been used for EMW feedstock experiments since 2021. Baseline soil samples were taken in 2021 before EMW amendment. As shown in **Figure 1**, four control plots were not amended with EMW feedstock, four plots were amended with various application rates of basalt feedstock (14.84, 11.10, 10.95, and 7.14 tonnes/acre), and four plots were amended with various application rates of steel slag feedstock (2.17, 2.04, 2.04, and 2.01 tonnes/acre). The mineralogical composition of the basalt and steel slag feedstock is described in the appendix. Further sampling was conducted in 2022, one year after field treatment. A soil corer was used to collect 12 soil samples at 20 meters apart from each of the 12 plots. Baseline samples were collected down to depths of 60 cm and post-amendment samples were collected to depths of 20 cm. Samples from each plot were pooled prior to measurement and analysis. A basalt feedstock sample and a steel slag feedstock sample were also analyzed according to the methods described below.

Haliburton Soil Sample Collection

Soil samples were taken from the Haliburton Forest and Wildlife Reserve in Ontario, Canada. Primarily a sustainably managed forest providing timber to the hardwood lumber industry, Haliburton Forest is also a research facility and education center. Four skid trails, each extending 500 meters up to 1 kilometer into the forest, were chosen by a team of researchers from Yale University and Trent University. Multiple locations were chosen along the skid trail to be sampled along a perpendicular transect of 12 meters. Each transect was sampled at three spots: directly on the skid trail (disturbed soil profile, compaction effects, etc.), 6 meters to the right of the skid train (relatively undisturbed), and 6 meters to the left of the skid trail (relatively undisturbed). 3 soil samples extracted from within a radius of 500 mm were composited to be representative of a single spot. For each soil sample, the top 10 cm of the soil profile, excluding the leaf litter and organic matter debris, was extracted with a bucket auger and then dried, ground, and sieved for analysis.

Elemental Analysis

Extracting Exchangeable Cations

All samples from both project sites were prepared for elemental analysis on a Thermo Scientific Element XR ICP-MS. 100 mg of dry soil was weighed out into acid-cleaned 15 mL centrifuge tubes. 12 mL of 1 M ammonium acetate was added to the sample, and to ensure complete leaching, centrifuge tubes were vigorously shaken for one minute, placed in a sonic bath, and sonicated for 10 minutes. Samples were centrifuged at 3600 rpm for 5 minutes. The ammonium acetate fraction was poured out, 2 mL of MQ water was added to each centrifuge tube, and tubes were shaken vigorously for one minute. Samples were centrifuged again at

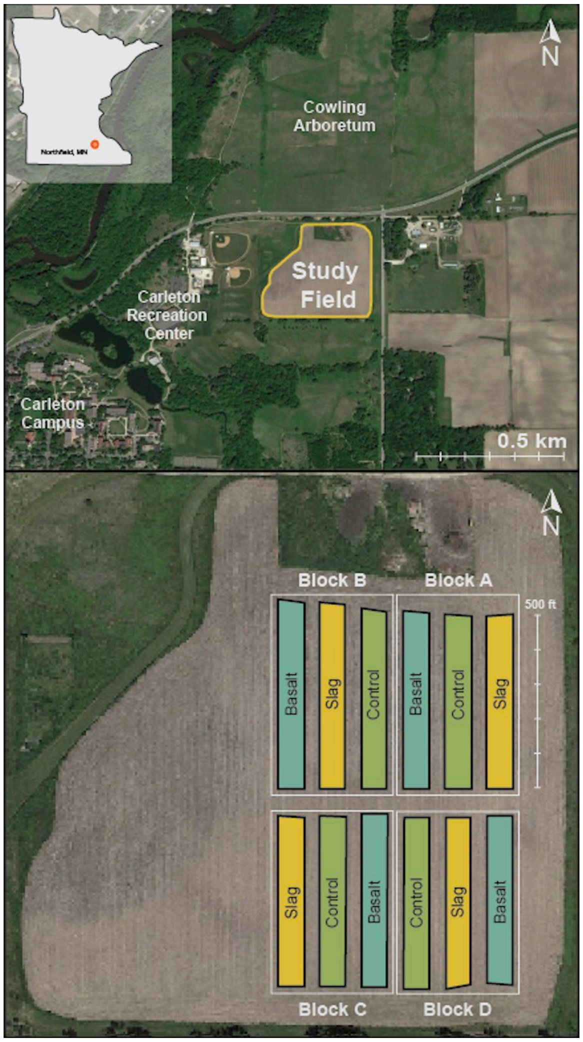

Figure 1*: Enhanced weathering trial setup at Carleton College, Northfield, Minnesota. Basalt and slag feedstock was applied at different rates in each plot.*

3600 rpm for 5 minutes. The MQ water fraction was poured out and the solid fraction was removed, placed into ceramic crucibles, dried overnight at 62°C, weighed, ashed overnight at 600°C, and weighed again. 41 mg of a USGS SGR-1b shale standard from the Green River Formation was ashed and prepared alongside each project site sample batch.

Total Acid Digest

Ashed soil samples were placed in Teflon beakers. At this stage, 14 mg of a USGS BHVO-2 basalt standard from the Hawaiian Volcanic Observatory was prepared with each sample batch. 5 mL of trace metal grade distilled HNO_3 and 5 mL of trace metal grade distilled HCl was pipetted into each beaker. Samples were left to rest in a closed fume hood for 1 hour before the addition of 1 mL HF to each beaker. Beakers were capped and placed on a hot plate overnight at 100°C. Samples were then uncapped and placed on a hot plate at 90°C until the liquid fraction evaporated. 5 mL of 6N HCL was added to each dry sample and beakers were placed on a hot plate for 1 hour at 65°C. After cooling, samples were transferred to 15 mL Nalgene bottles.

Isotope Spike Cocktail

Isotope spike powders of $CaCO_3$, MgO, and TiO_2, synthetically enriched in the isotopes ^{42}Ca, ^{26}Mg, and ^{49}Ti were purchased from Isoflex USA. The powders were dissolved using the total digest method, with the Ti requiring an additional HF addition step. After the digest, the solutions were evaporated and brought up in 5% HNO_3. An isotope spike cocktail containing 232 ppm Ca, 260 ppm Mg, and 166 ppm Ti was prepared from splits of each of the solutions.

10 µL of sample was pipetted into Teflon beakers and placed on a hot plate at 85ºC for about 1 hour, until evaporated. 5 µL of isotope spike cocktail was added to each beaker. Samples were placed on a hot plate at 85ºC for about 30 minutes, until evaporated. 4 mL of 5% HNO_3 with 1 ppb Indium (used as an internal standard) was pipetted into each beaker. Teflon beakers were capped and placed on a hot plate at 65ºC for 1 hour, pipetted into 4 mL acid-cleaned plastic vials, and centrifuged at 4000 rpm for 5 minutes. Additional blanks were prepared from 5% HNO_3 with 1 ppb Indium. After preparation, all samples were run on a Thermo Scientific Element XR ICP-MS.

Elemental Analysis Data Reduction

Average Indium intensities (measured in counts per second) for each of three Element ICP-MS modes used (standard, and oxygen and helium KED) were used to normalize average intensities for each element according to the equation:

$$Normalized\ element =$$

$$\frac{Sample\ element * Average\ Indium\ for\ sample\ mode}{Sample\ Indium}$$

For each block of samples in the ICP-MS run, the average element count of prepared blanks was subtracted from the element count of both geostandards and samples, for each element measured. Next, element concentration was calculated with two methods. The standard method was used for elements not contained in the isotope spike, and the isotope dilution method was used for elements contained in the spike (Ca, Mg, and Ti).

Standard Method

Varying concentrations of a bespoke shale standard from Isoflex USA containing all elements of interest were run with samples on the ICP-MS and a calibration curve was created, yielding a linear plot of average intensity vs. concentration, for each element analyzed. After confirming that the R^2 values of these plots were sufficiently high ($R^2 > 0.96$), elemental concentration in units of ppm was calculated by multiplying the element count by the shale standard calibration curve slope, for each element. The total amounts of each element in the digested samples were obtained by multiplying the ppm concentration of each element by 400, the dilution factor from the mother solution (6 N HCl solution) to ICP-MS-run samples.

A geostandard correction was applied to both the BHVO2 basalt standard and the SGR-1b shale standard. Known concentrations of each element in both geostandards were divided by measured concentrations, for each element. Resulting values were averaged to calculate corrected BHVO2 and SGR-1b elemental concentrations. The geostandard with an average corrected value closest to 1.0 was used as the correcting geostandard. Corrected elemental concentrations in digested samples were calculated by multiplying measured values by the value of the correcting geostandard.

Corrected elemental concentrations of digested samples were coupled with the volume of mother solution and weight of soil samples to obtain concentration values of each element in the soil samples. This method of isotope dilution is a highly accurate and common way of obtaining element concentrations in a range of natural samples (Evans and Clough, 2005; Stracke et al., 2014).

Isotope Dilution Method

Concentrations of the elements Ca, Mg, and Ti were calculated by constructing a series of equations relating isotope spike element values and ICP-MS measured values. Atom counts of elemental isotopes in the isotope spike cocktail are known, as are measured elemental isotope counts and ratios. Thus, taking the example of Ca, $(^{40}Ca/^{42}Ca)_{measured}$ and $(^{40}Ca/^{42}Ca)_{spike}$ are known ratios ($R_{measured}$ and R_{spike}). Incorporating the equations

$$^{40}Ca_{measured} = {}^{40}Ca_{natural} + {}^{40}Ca_{spike}$$

and

$$^{42}Ca_{measured} = {}^{42}Ca_{natural} + {}^{42}Ca_{spike}$$

yields a system of 4 equations with 4 unknowns which can be solved for the total number of Ca atoms. Continuing with the example above, the amount of $^{40}Ca_{natural}$ is calculated according to the equation:

$$^{40}Ca_{natural} = \frac{^{40}Ca_{measured} - (R_{spike} * {}^{42}Ca_{measured})}{1 - \frac{R_{spike}}{R_{sample}}}$$

Once this value is obtained, the isotopic concentration of each element can be calculated according to the equation:

$$^{40}[Ca]_{natural} = \frac{[Ca]_{stock\ spike\ cocktail}}{Dilution\ factor_{spike}} * \frac{^{40}Ca\%_{spike}}{^{40}Ca\%_{natural}} * \frac{^{40}Ca_{natural}}{^{40}Ca_{spike}}$$

Elemental concentration in ppm of digested sample was extrapolated to elemental concentration of soil samples via the calculations described in the standard method. The isotope dilution method was applied to calculate the total number of Ca, Mg, and Ti atoms.

Total Organic Carbon/Total Inorganic Carbon

Total carbon and total inorganic carbon were measured on an ELEMENTRAC CS 580 elemental analyzer for all 39 samples across the two project sites. Total carbon was measured by combusting 200 mg of soil sample in a reactive chamber up to 1350 ºC. Total inorganic carbon was measured by diluting 200 mg of soil sample with 2 g nanopure water and reacting with 6 mL 1.5 M HCl. NIST calcium carbonate standards were run alongside samples to ensure instrument precision.

Soil pH

Dry soil samples were sieved through a 2 mm sieve and 10 g of each sample was weighed out into 50 mL falcon tubes. 10 mL of milliq2 water was added to each sample and samples were shaken vigorously for 1 minute and left to rest for 10 minutes. Soil pH was measured with an Orion StarTM A121 Portable pH Meter with the OrionTM ROSSTM Sure-FlowTM pH Electrode.

Sikora Buffer pH

The Sikora buffer pH method was used to measure sample buffering capacity (Sikora, 2006). 10 mL of Sikora buffer solution was added to each soil-water sample slurry and samples were shaken in an Eberbach shaker table for 10 minutes at 180 oscillations per minute. pH was measured again with the same pH probe, and buffer pH calculated.

RESULTS

Alternative Feedstock

Soil concentrations of the mobile elements Na, Mg, and Ca are expected to remain constant in control plots and decrease after initial feedstock addition in basalt-amended and slag-amended plots as weathering processes dissolve feedstock and mobile cations are transported by groundwater or riverine systems away from the field site. Na, Mg, and Ca supplied to the soil by feedstock application are generally water-soluble. These elements can be taken up as cations by biologic systems, including plant roots, and can be exchanged among mineral phases. Minerals containing Si, Na, Mg, and Ca are generally chemically instable and undergo weathering in natural environments (Riebe et al., 2003). Additionally, these mobile elements can form secondary minerals. Secondary mineral formation in soil, though capable of sequestering CO_2 in forms such as $CaCO_3$, inhibits the full potential of EMW carbon capture by preventing the transport of dissolved alkalinity in the form of bicarbonate to the ocean. Without secondary mineral formation, Ca^{2+} and HCO_3^- combine to sequester two moles of CO_2 for every mole of reacted feedstock, forming stable carbonate minerals that are stored permanently by burial under the sea floor (Vibbert and Park, 2022). At neutral pH, the net reaction is:

$$CaSiO_3 + 2H_2O + 2CO_2 \rightarrow Ca^{2+} + 2HCO^{3-} + SiO_2 + H_2O$$

Soil concentrations of immobile elements Ti and Th are expected to remain constant in control plots and increase past baseline values in basalt-amended and slag-amended plots due to the deposition of trace metals from feedstock sources into the soil (Reershemius et al., 2023). Ti and other elements such as Th, Zr, Nb, and Ta are ideal immobile element tracers because they are primarily contained in minerals which are resistant to weathering. Ti is considered insoluble in soil because its host minerals, such as rutile, are chemically stable (Brimhall et al., 1991; Ayers and Watson, 1993; White, 1995; Reershemius et al., 2023). Furthermore, Ti is shown to lose mobility above the nanometer-scale (Tilley and Eggleton, 2005). Elemental concentrations in control, basalt-amended, and steel slag-amended soil samples did not change homogeneously after feedstock application, as shown in **Figure 2**. Furthermore, elemental concentrations in control plots did not remain constant between years 2021 and

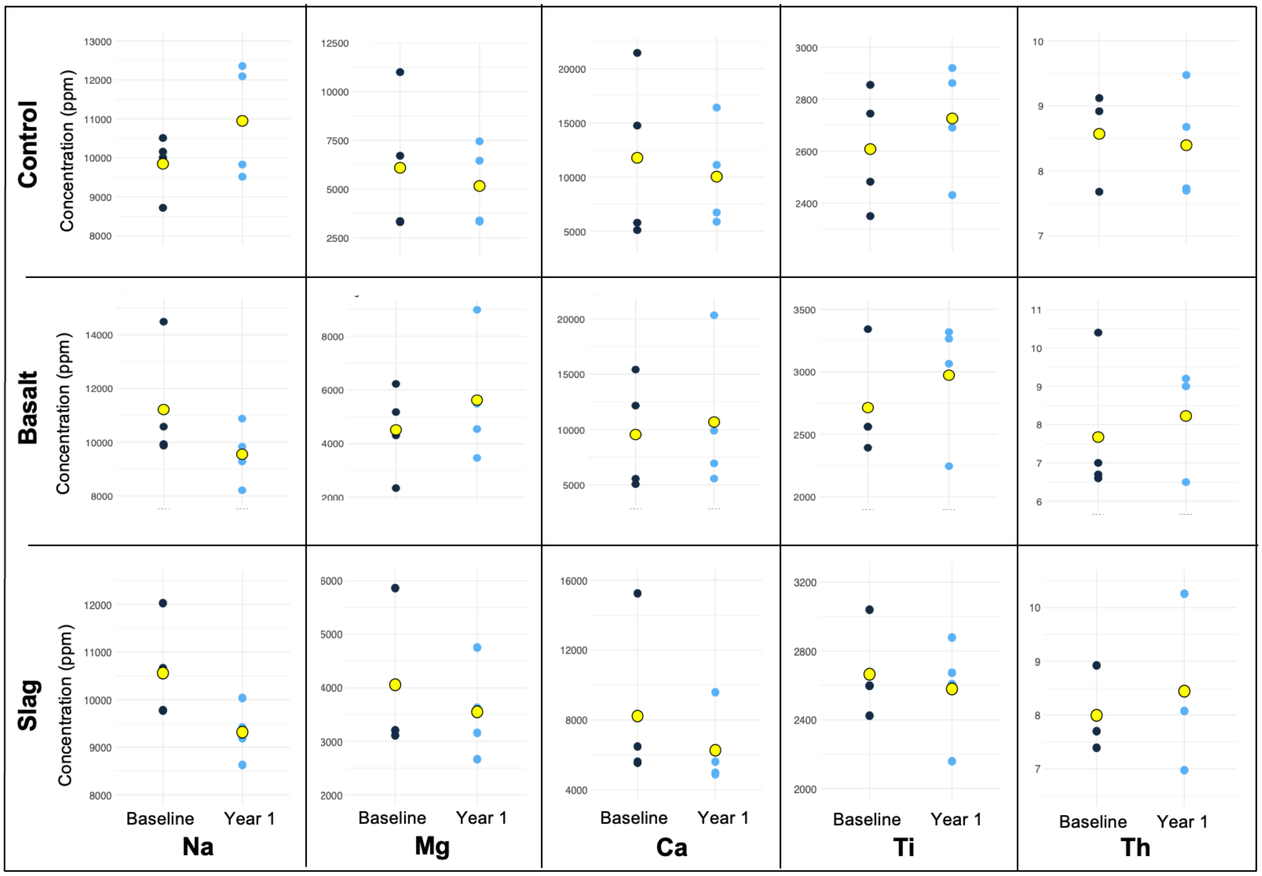

Figure 2: Pre- and post-feedstock amendment soil elemental concentrations in control, basalt-amended, and slag-amended plots at Carleton College, Northfield, Minnesota. Yellow points mark the average elemental concentration between four plots.

2022. Because elemental concentrations did not change in one direction, either among element or among field plot type, I conclude that environmental factors between sampling years did not unidirectionally influence the sampling results. Instead, the TiCAT method can be used to make interpretations of this unanticipated data.

Given a sufficiently granular spatial sampling regime, the TiCAT method can be used to approximate the rate of CDR via enhanced weathering. The baseline soil composition and applied feedstock compositions are plotted by immobile element (Ti) and mobile element (Na, Mg, or Ca) concentrations, with the linear trendline forming a homogeneous mixing line. A post-feedstock amendment soil sample, assumed to consist of a homogenous mixture of baseline soil and feedstock, is plotted and the change in mobile cation concentration is calculated as the distance below the homogeneous mixing line, assuming [Ti] remains constant (Reershemius et al., 2023). **Figure 3** visualizes this method.

It is possible to calculate expected elemental values after one year of EMW field treatment using a simple mass balance approach. This is done by using the known values of feedstock application rate, baseline soil elemental concentrations, and basalt and slag compositions to estimate the soil density, basalt and slag densities, and mixing depth of feedstock, assuming homogeneous and complete mixing. Table 1 in the appendix describes the results of these calculations, which are visualized in **Figure 4**.

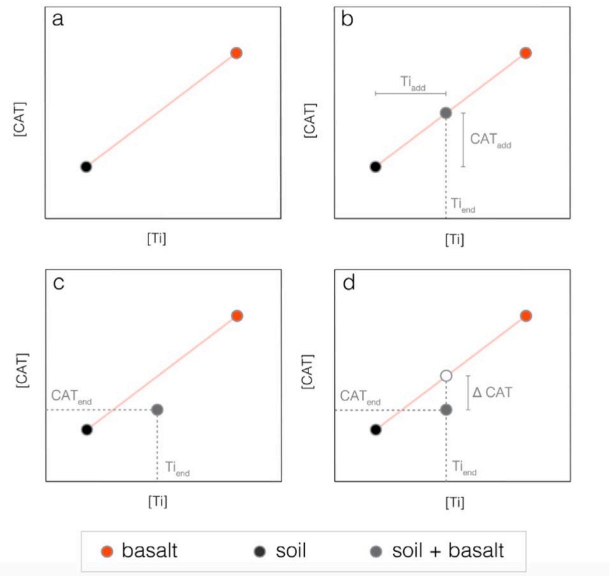

***Figure 3**: The TiCAT conceptual framework as a simple two-component mixing model. (a) An idealized soil and basalt endmember are plotted in Ti v CAT space. (b) A mixture of soil+basalt initially plots on the idealized mixing line between both endmembers. c) Dissolution results in loss of CAT from the solid phase, while Ti is conserved as it is immobile. (d) The original composition of the soil+basalt mixture (indicated by the white circle) is the intersection of Tiend with the mixing line; ΔCAT is the amount of CAT lost by dissolution. (From Reershemius et al., 2023).*

As **Figure 5** demonstrates, in some plots and for some elements, measured soil elemental concentration values are higher than expected. In other plots and for other elements, values are lower than expected. In basalt-amended and slag-amended plots, $[\text{Na}]_{\text{measured}} < [\text{Na}]_{\text{expected}}$ and $[\text{Mg, Ca}]_{\text{measured}} > [\text{Mg, Ca}]_{\text{expected}}$. With the exception of elemental concentrations from one basalt-amended plots, $[\text{Ti, Th}]_{\text{measured}} > [\text{Ti, Th}]_{\text{expected}}$. Control plots change in both directions across all elements measured, indicating that field-scale environmental changes from the year 2021 to the year 2022 such as the application of fertilizer or heavy rainfall are not the source of differences between measured and expected elemental concentration values.

Though percent error is low (Na: ± 0.546%, Mg: ± 0.191%, Ca: ± 0.428%, Ti: ± 0.098%, Th: ± 0.195%), the lack of data stability between sampling years in control plots indicates a need for greater spatial granularity in soil sampling. Soil samples from Carleton College in Minnesota were collected every 20 meters but pooled for each plot, increasing the representative area of one measured sample from 400 m^2 to 57,600 m^2. Because

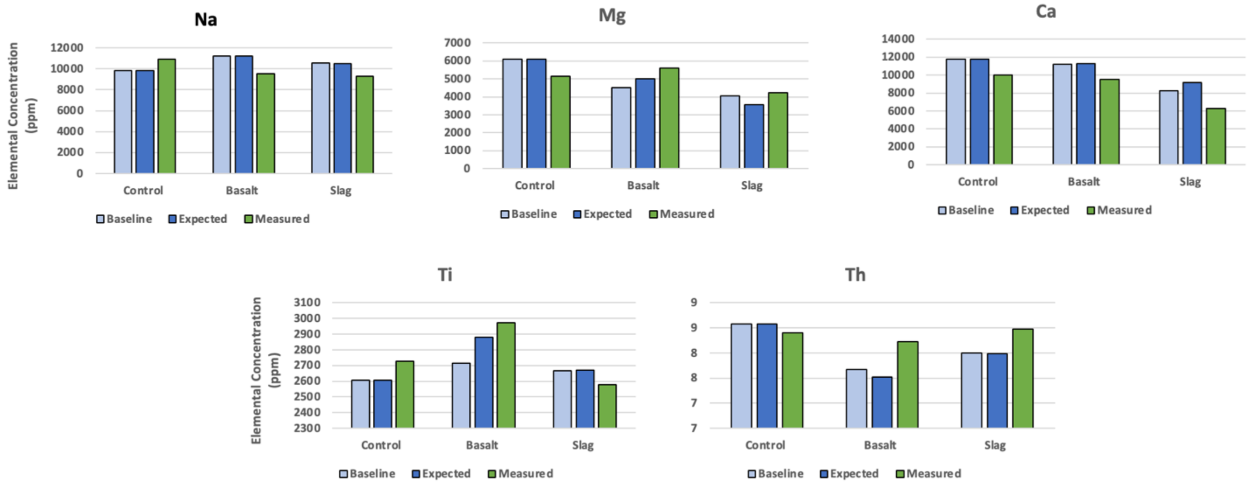

***Figure 4:** Baseline, expected, and measured soil elemental concentrations for control, basalt-amended, and steel slag-amended plots from Minnesota. Expected values were calculated using a mass balance approach, coupling inputs of feedstock application rate, baseline soil elemental concentrations, and basalt and slag compositions.*

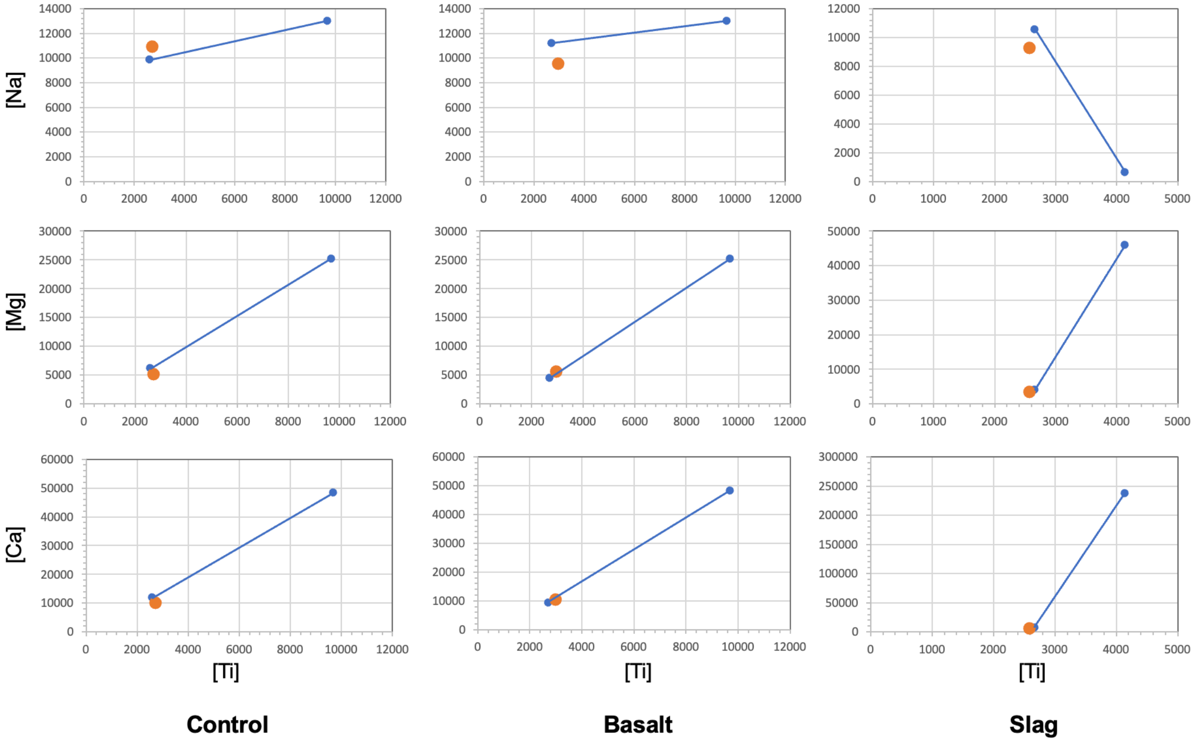

Figure 5: Elemental concentrations (ppm) of Ti plotted against Na, Mg, and Ca cations for control, basalt, and slag fields at Carleton College, Northfield, Minnesota, following the TiCAT conceptual framework. The blue line represents the homogeneous mixing line between baseline soil composition (lower [Ti]) and pure feedstock composition (higher [Ti]). Post-feedstock amendment soil sample elemental concentrations are plotted in orange.

control plots display heterogeneously changing soil element concentrations, indicating a variable baseline, basalt and slag-amended field CDR rates cannot be accurately calculated from the data collected. Attempts to calculate CDR rates of basalt and slag-amended fields failed due to inconclusive and/or unresolved data. ICP-MS elemental concentration data was plotted according to the TiCAT framework, but most post-amendment samples did not fall into the expected elemental concentration range. As shown in **Figure 3**, it is expected that [Ti] is higher than baseline soil values and lower than feedstock values and that [Na, Mg, Ca] falls below the homogeneous mixing line but above baseline soil values. In our sample suite, however, post-amendment samples fail to meet expectations as [Na, Mg, Ca] falls below baseline soil values, [Na, Mg, Ca] and [Ti] fall very near the baseline soil composition, or the sample plots above the homogeneous mixing line.

There are several phenomena, visualized in **Figure 6**, which can explain this collected data. Competing geochemical effects may cause cations dissolved from feedstock minerals to precipitate as secondary minerals instead of being removed from the field site. In this case, post-amendment sample data plots above the homogeneous mixing line (Reershemius et al., 2023). This result occurs when Na is used as a tracer in the control plots and Mg is used as a tracer in the basalt-amended plots.

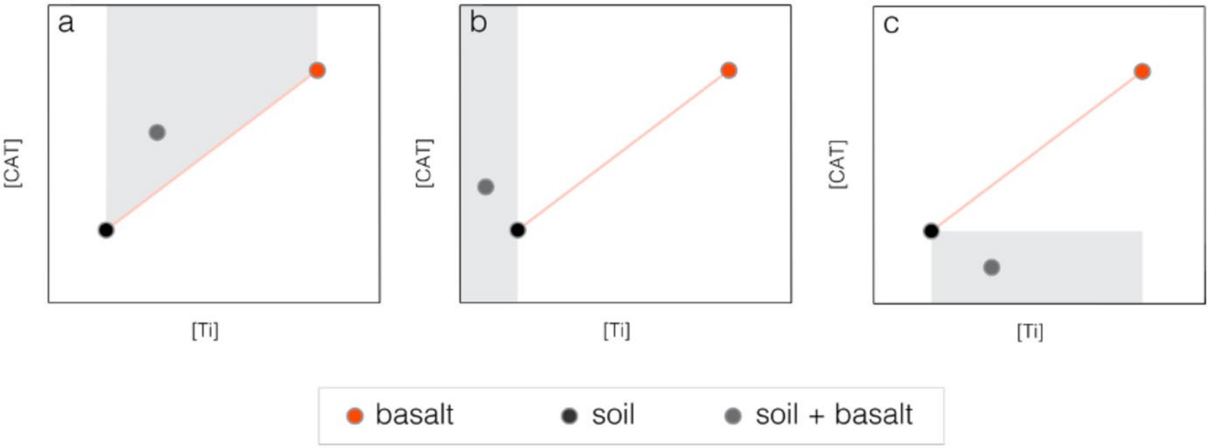

Figure 6: *Cases where the composition of soil+basalt mixtures fall outside of the TiCAT framework: (a) $\Delta[CAT] < 0$, indicating precipitation of CAT into a secondary mineral phase; (b) $[Ti]end < [Ti]soil$, indicating the soil baseline value for Ti is not suitable; (c) $[CAT]_{end} < [CAT]_{soil}$, indicating dissolution of CAT from soil. (From Reershemius et al., 2023).*

If $[Ti]_{post\text{-}amended} < [Ti]_{baseline\ soil}$, the baseline soil data is not suitable. The most likely instance of this case is when soil sampling practices do not accurately reflect natural soil spatial variability (Reershemius et al., 2023). If too few locations are sampled in a field, or if too many samples are pooled together for analysis, post-amendment soil sample data cannot be directly compared to baseline soil values. This result occurs when Na, Mg, and Ca are used as tracers in the slag-amended plots.

Finally, a result of $[Na, Mg, Ca]_{post\text{-}amended} < [Na, Mg, Ca]_{baseline\ soil}$ indicates that these cations have dissolved from the soil in addition to the feedstock (Reershemius et al., 2023). In this situation, mineral weathering has occurred but CDR rates cannot be calculated because the fractionation of dissolution between soil and feedstock is not known. Attempting to calculate CDR rates with this data runs the risk of overestimating CDR. This result occurs when Mg and Ca are used as tracers in the control plots and Na is used as a tracer in the basalt-amended plots. The only sample falling within the expected TiCAT framework range is the Ca-tracer basalt sample. However, the post-amended sample plots close to the baseline sample, indicating that the applied basalt may have not fully mixed into the soil and the scale of carbon sequestration is not significant.

It is inconclusive if the use of steel slag as an agricultural EMW feedstock produces CDR rates comparable to those of basalt. All three choices of mobile cation tracers yielded results outside of the TiCAT framework's expected range and CDR rates cannot be calculated. As described above, baseline soil samples do not reflect the extent of field-scale soil heterogeneity when $[Ti]_{post\text{-}amended} < [Ti]_{baseline\ soil}$, making them unsuitable for comparison with post-amendment samples. If EMW on agricultural fields is to be deployed at any scale in the coming years and decades, CDR rates must be calculated with high accuracy. To ensure quality and high confidence in calculated CDR rates, soil sampling regimes must be sufficiently spatially granular. The exact spatial dimensions of sufficient sampling will vary with geographic region and environmental factors, but the following analysis aims to establish a framework for determining the number of baseline and post-feedstock amendment soil samples that must be collected within a given EMW deployment area.

Spatial Sampling Variability

To determine the number of soil samples that must be collected to sufficiently account for spatial soil heterogeneity at the field sites, I conducted a statistical analysis of baseline soil samples from Haliburton Forest in Ontario, Canada and extended the analysis and data visualization to baseline and post-feedstock amendment soil samples from Minnesota. As shown in **Figure 7**, elemental concentrations from the Haliburton sample set displayed higher variability between sampling locations, among most elements, despite representing a smaller field area per sample (400 m^2 for Haliburton samples and 2787 m^2 for Minnesota samples). Therefore, I assume that any method applied to the Haliburton Forest sample set can be accurately translated to the Minnesota sample set.

A simple statistical model can produce recommendations for the number of samples required to capture natural soil elemental variation. I assumed that the mean of the 15 soil samples from Haliburton Forest approximates the true mean of the sampling area for each element studied. This assumption created a partial limitation on our study, but I proceeded with this method because Haliburton Forest soil samples were collected at a greater spatial granularity than standard agronomic practice.

A normal distribution was created from the mean and standard deviation of the Haliburton Forest sample set. Taking subsets of numbers from this normal distribution, mean values of n number of samples were calculated for $n \leq 50$. Finally, deviations of these means from the true mean were calculated and plotted against the value of n. This statistical simulation was run 100 times to generate the plots in **Figure 8**, which can inform spatial sampling decisions.

Among all mobile and immobile elements studied, the sharpest decrease in variance occurs when $0 < n < 5$. However, in most runs, variance undergoes a general leveling off at around n = 25-30 samples averaged. This suggests that the original sample set of 15 insufficiently captured natural variation in soil composition. For future work on the Haliburton Forest wollastonite EMW trial, double the number of samples should be collected at each trial site so that spatial sampling regimes increase in granularity.

It should be noted that the application rate of EMW feedstock will determine an acceptable level of uncertainty in soil elemental

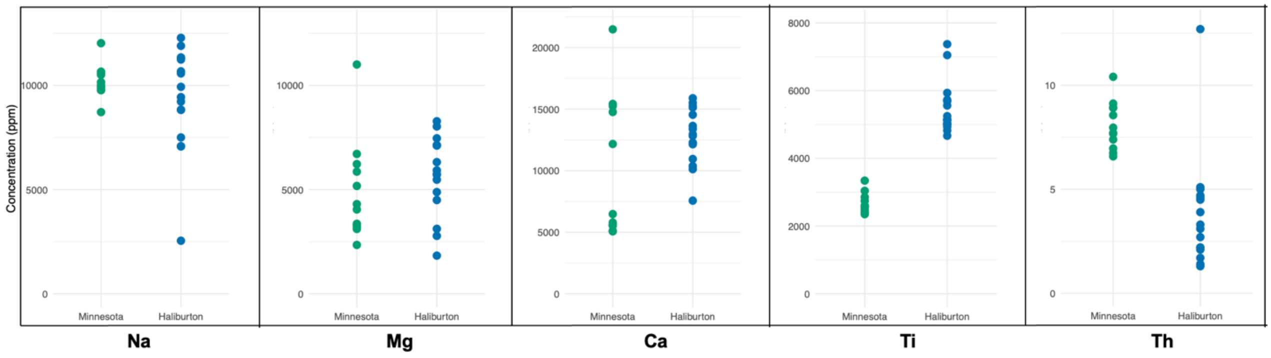

Figure 7: *Spread of baseline elemental concentrations in soil sample sets from Carleton College, Minnesota, USA and Haliburton Forest, Ontario, Canada.*

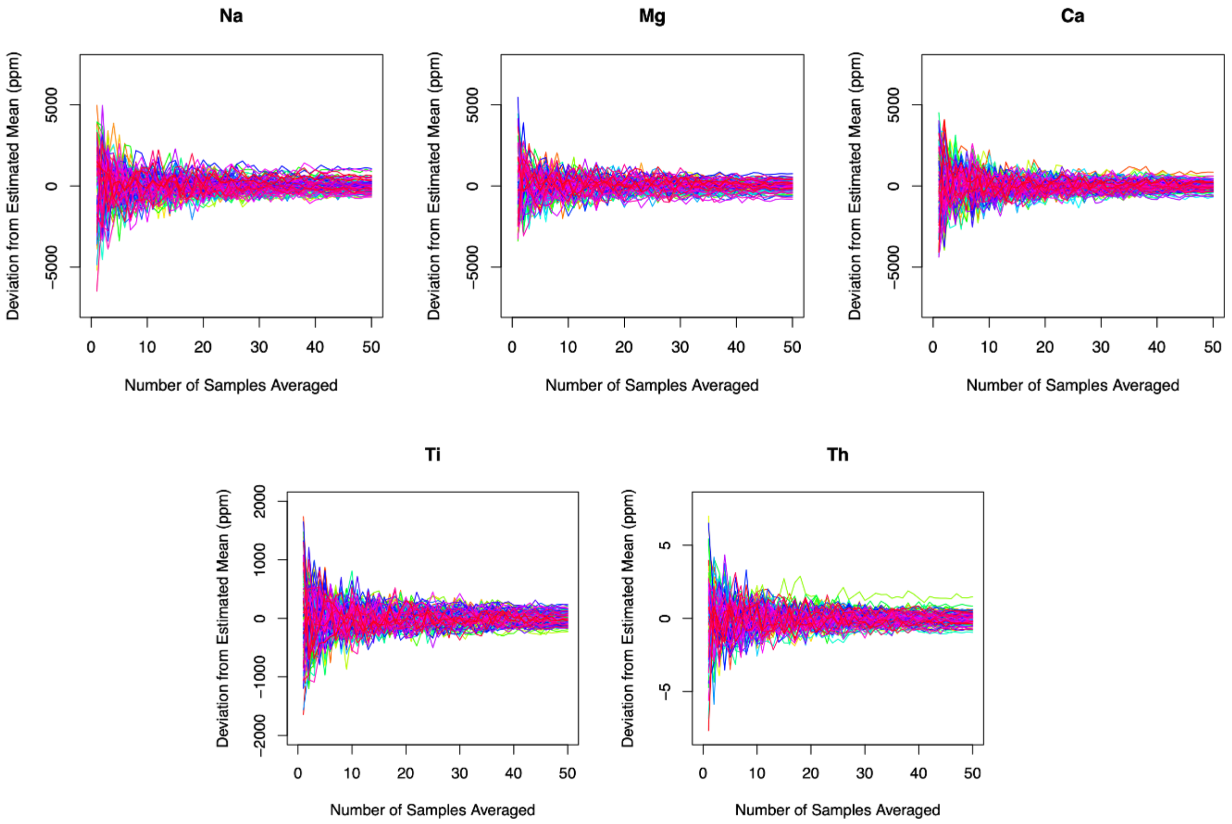

Figure 8: Spatial statistical analysis of Haliburton Forest baseline soil samples, where the x-axis represents the number of averaged values and the y-axis represents deviation from the estimated mean, which is approximated as the true mean. This statistical simulation was run 100 times, with each simulation output in a different color.

concentrations. With high application rates, the amount of each study element added to the soil by feedstock addition is far greater than baseline soil samples' deviation from the true mean. In this case, uncertainty decreases as the value of estimated deviation is much smaller than the value of elemental addition. However, when feedstock application rate is low, acceptable levels of uncertainty from statistical modeling must decrease to retain confidence.

Baseline soil samples from the Minnesota basalt/slag EMW trial were run on the same statistical model and results shown in **Figure 9** reveal a spatial trend remarkably similar to the Haliburton Forest sample set, with sharpest decrease in variance happening when $0 < n < 5$ and another leveling-off when $n = 25$-30.

These results are corroborated when Minnesota basalt/slag EMW post-feedstock amendment samples are subjected to the same statistical analysis, visualized in **Figure 10**. Once again, deviation from the estimated mean decreases when $n = 25$-30, indicating that standard agronomic sampling practices yielded a sample size (12) insufficiently spatially granular for EMW MRV purposes.

It is important to note that when using this method, researchers can choose an acceptable level of uncertainty in soil elemental concentrations. However, EMW deployment in the real world requires that factors such as time, cost, and labor for sampling be minimized. It will be a question for carbon offset registries and independent carbon capture project verifiers to institute an accepted maximum value of uncertainty

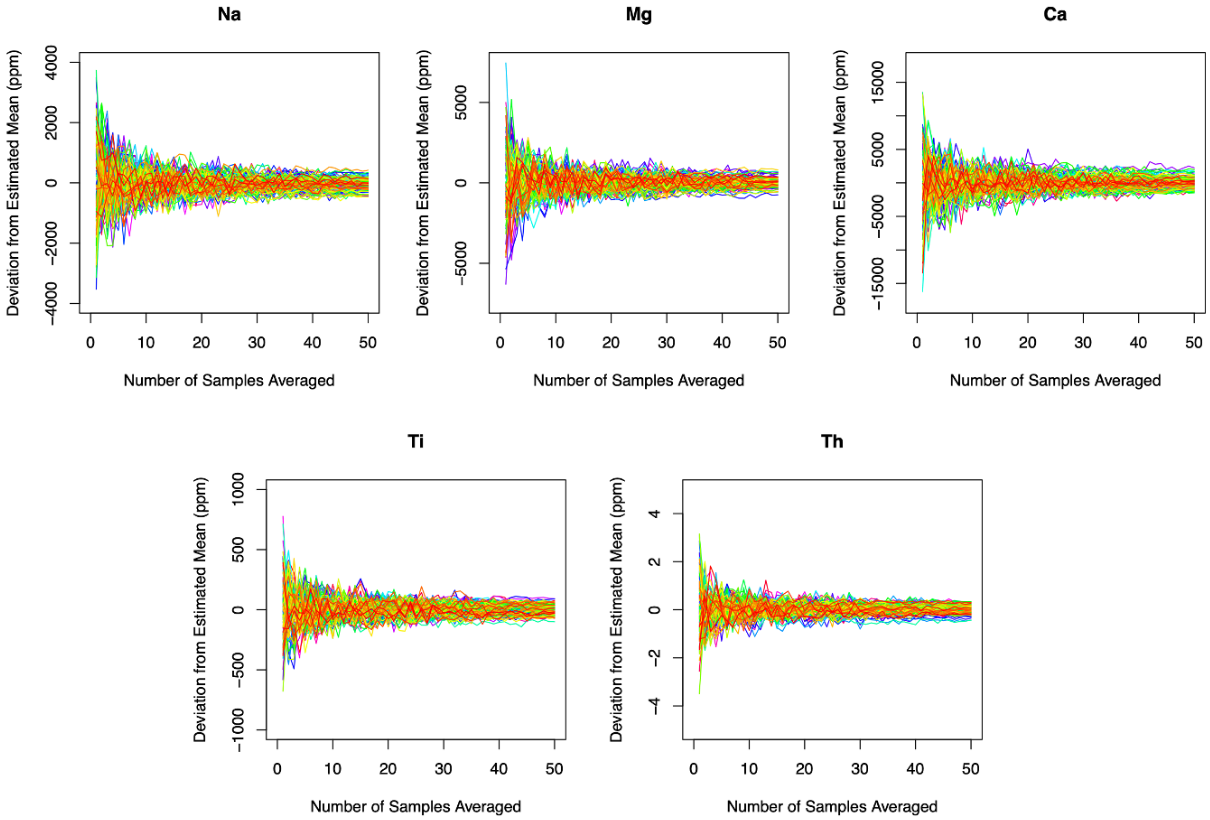

Figure 9: *Spatial statistical analysis of Minnesota baseline soil samples, where the x-axis represents the number of averaged values and the y-axis represents deviation from the estimated mean, which is approximated as the true mean. This statistical simulation was run 100 times, with each simulation output in a different color.*

when measuring soil elemental concentration, as this will have consequences when calculating rates of carbon dioxide removal for MRV.

FURTHER CONSIDERATIONS

EMW Co-benefits

The scope of this project did not include a study on the effects of EMW practices on soil health and crop yield. However, other studies have shown that the addition of basalt to cropland increases sugarcane yields by up to 29% (Beerling et al., 2018) and corn and wheat yields by up to 7 ± 4.3% in field scale trials (Guo et al., 2023). Application of wollastonite to soybean and rye plants in laboratory trials created a 41-200% and 72% increase in yield (Haque et al., 2020; Jariwala et al., 2022). The addition of potassium, phosphorous, and micronutrients to the soil from feedstock application increases both crop yield and growth rate while reducing fertilizer use (Puro.earth, 2022). EMW trials using basalt and wollastonite feedstock have been shown improve overall soil health by decreasing soil acidity in a manner similar to standard lime treatment on agricultural land (Gillman et al., 2001, 2002; Anda et al., 2015). Steel slag EMW trials are fewer in number, but preliminary studies suggest that slag amendment on agricultural fields produces similar results (Das et al., 2019; Deus et al., 2020).

In addition, EMW deployment may increase job opportunities across the United States, especially in agricultural regions which are most likely to suffer from the effects of

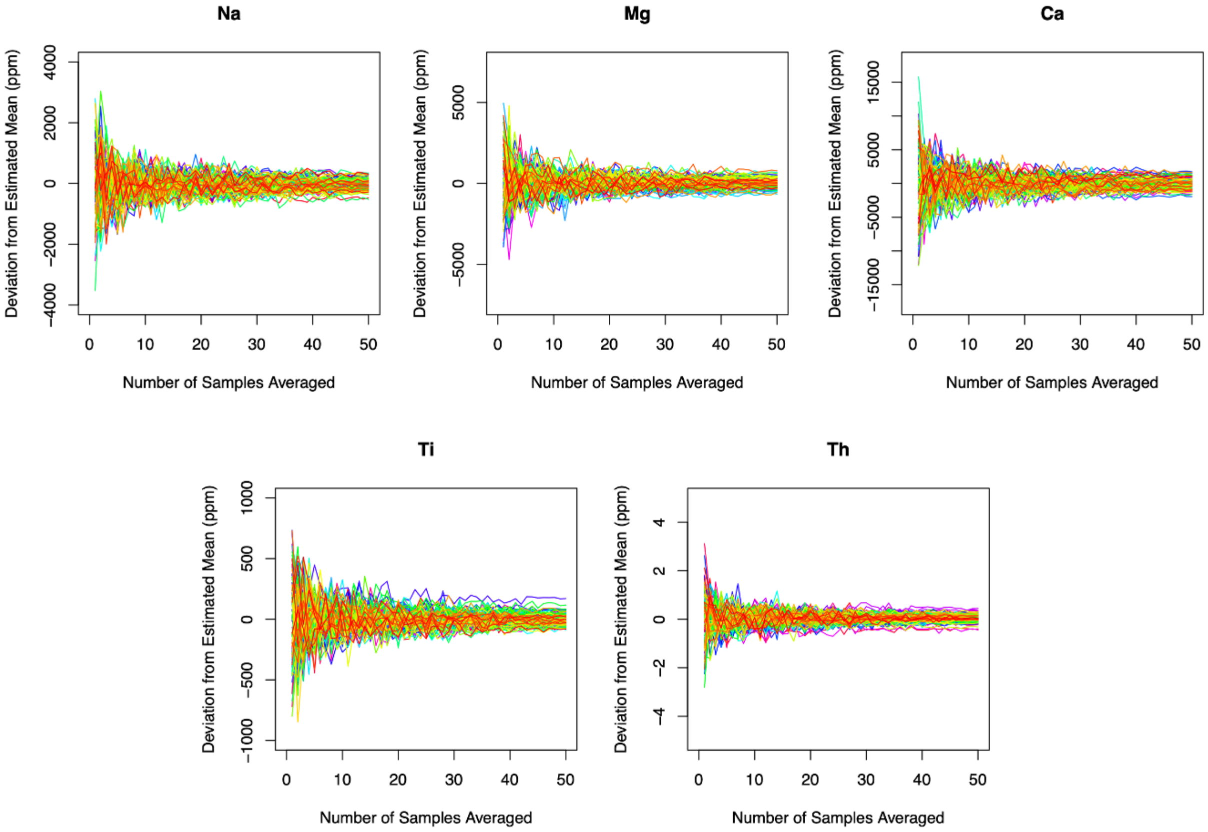

Figure 10: *Spatial statistical analysis of Minnesota post-feedstock amendment soil samples, where the x-axis represents the number of averaged values and the y-axis represents deviation from the estimated mean, which is approximated as the true mean. This statistical simulation was run 100 times, with each simulation output in a different color.*

climate change. More investigation of the potential environmental justice and human health impacts of EMW practices is required before these projects can fully scale.

EMW Environmental Harms

The procurement of rocks required for large-scale EMW deployment may be an energy-intensive process. Rocks must be mined and ground down to a small size, with millimeter-scale diameter maximizing the surface area of the material and increasing the efficacy of carbon removal. The feedstock mining, grinding, and transportation process will decrease the amount of net negative emissions that a given EMW project can claim. Life cycle assessments should be conducted for each EMW project and factored into carbon credit claiming to ensure a net negative cradle-to-grave process.

MRV for EMW

Existing carbon offset methodologies center heavily on biologic carbon removal solutions such as reforestation and afforestation. The first (and only, to date) EMW carbon removal methodology was published by Finnish registry PuroEarth in 2022 (Puro.earth, 2022). The methodology outlines principles for verifiable EMW projects, such as the creation of an environmental risk assessment and life cycle assessment, safe sourcing of feedstock, and continued field measurements which last for the duration of the project. At the same time, it states that a "general scientific consensus on best practice of simulation and associated MRV does not yet exist." The PuroEarth methodology does not provide guidance or regulation about which EMW MRV methods acceptably constrain CDR rate uncertainties. Beyond conducting a soil analysis to establish the baseline soil profile and a geochemical assay to establish the composition of the feedstock, project verifiers may proceed with one of multiple MRV strategies. Moving forward, scientific research should inform future EMW methodology development and refinement by making an MRV approach recommendation to constrain carbon removal rate estimates and prevent the overcounting of carbon credits claimed.

CONCLUSION

The CDR rates of enhanced weathering in Minnesota basalt and steel slag-amended agricultural plots could not be calculated due to insufficiently sampled baseline soils. Though the mass spectrometry data used to calculate the elemental concentrations of mobile (Na, Mg, Ca) and immobile (Ti, Th) elements was low in percent error (under ± 0.546%), changes in cation concentrations fell outside the range of expected values when the TiCAT framework method was applied. The elemental concentrations of all studied elements in the control plots did not remain stable and the measured elemental values in basalt and slag-amended plots changed heterogeneously from expected values, indicating that baseline soil samples were not accurately representative of true spatial elemental variation in the plots. Thus, further research should be conducted to determine if steel slag is an effective substitute for basalt in EMW carbon capture projects.

To support the development of MRV for EMW projects and modify sampling procedures for the ongoing Minnesota EMW trial, a statistical simulation was run on Haliburton Forest baseline soil samples and Minnesota baseline and post-feedstock amendment soil samples. Results indicate that previous sampling practices yielded sample sets with high deviation from true elemental means. For both sample sets, model results suggest that the size of the sample set be increased to 30 samples. This method can be incorporated into MRV methodology development, where carbon offset registries can specify an acceptable level of uncertainty in baseline soil elemental values to further constrain CDR rate estimates.

The scientific community should continue to develop studies on soil health and crop-yield co-benefits, environmental harms, human health risks, and registry methodology development associated with EMW. As enhanced weathering startups such as Lithos, Eion, Undo, Verde AgriTech, Vesta, greenSand, Silicate Carbon, and others begin to generate carbon offset credits, rigorous field-scale empirical data collection is all the more important. The research of co-benefits, harms, lifecycle emissions, and MRV strategies should grow alongside EMW projects as EMW deployment continues to scale.

ACKNOWLEDGMENTS

I am grateful for the ongoing support and encouragement of my advisors, colleagues, family, and friends. Thank you to Noah Planavsky for introducing me to carbon capture concepts and geochemistry laboratory research during my sophomore year; I greatly appreciate your guidance throughout this work. Thank you to Michael Oristaglio for sparking my interest in climate change solutions and for encouraging me in my career and personal development. Thank you to EPS graduate students and post-docs who supported me in every aspect of laboratory research and data analysis during my time at Yale: Brian Beaty, Abby Lunstrum, Ella Holme, Nico Theunissen, Isabella Chiaravalloti, Ella Milliken, Chloe Kent, Gryphen Goss, and Sam Shipman. I especially appreciate the guidance of graduate students Tom Reershemius and Ayesha Ahmed in the development and refinement of this project, without whom the creation of this manuscript would not have been possible. I am thankful for the encouragement of my fellow EPS undergraduates and Club Geo members and for our shared memories in the department. Thank you to my friends in Trumbull College and Christian Union for supporting me in my personal and academic life this semester and to my family for cheering me on from afar. Lastly, I owe all my gratitude to God for sustaining me in every way.

REFERENCES

Almaraz M., Bingham N. L., Holzer I. O., Geoghegan E. K., Goertzen H., Sohng J. and Houlton B. Z. (2022) Methods for determining the CO2 removal capacity of enhanced weathering in agronomic settings. *Front. Clim.* **4**.

Amann T. and Hartmann J. (2022) Carbon Accounting for Enhanced Weathering. *Front. Clim.* **4**.

Anda M., Shamshuddin J. and Fauziah C. I. (2015) Improving chemical properties of a highly weathered soil using finely ground basalt rocks. *CATENA* **124**, 147–161.

Ayers J. C. and Watson E. B. (1993) Rutile solubility and mobility in supercritical aqueous fluids. *Contrib. Mineral. Petrol.* **114**, 321–330.

Beerling D. J., Kantzas E. P., Lomas M. R., Wade P., Eufrasio R. M., Renforth P., Sarkar B., Andrews M. G., James R. H., Pearce C. R., Mercure J.-F., Pollitt H., Holden P. B., Edwards N. R., Khanna M., Koh L., Quegan S., Pidgeon N. F., Janssens I. A., Hansen J. and Banwart S. A. (2020) Potential for large-scale CO2 removal via enhanced rock weathering with croplands. *Nature* **583**, 242–248.

Beerling D. J., Leake J. R., Long S. P., Scholes J. D., Ton J., Nelson P. N., Bird M., Kantzas E., Taylor L. L., Sarkar B., Kelland M., DeLucia E., Kantola I., Müller C., Rau G. and Hansen J. (2018) Farming with crops and rocks to address global climate, food and soil security. *Nat. Plants* **4**, 138–147.

Brimhall G. H., Christopher J. L., Ford C., Bratt J., Taylor G. and Warin O. (1991) Quantitative geochemical approach to pedogenesis: importance of parent material reduction, volumetric expansion, and eolian influx in lateritization. *Weather. Soils* **51**, 51–91.

Chilingar G. V., Sorokhtin O. G., Khilyuk L. and Gorfunkel M. V. (2009) Greenhouse gases and greenhouse effect. *Environ. Geol.* **58**, 1207–1213.

Chukwuma J. S., Pullin H. and Renforth P. (2021) Assessing the carbon capture capacity of South Wales' legacy iron and steel slag. *Miner. Eng.* **173**, 107232.

Das S., Kim G. W., Hwang H. Y., Verma P. P. and Kim P. J. (2019) Cropping With Slag to Address Soil, Environment, and Food Security. *Front. Microbiol.* **10**.

Deus A. C. F., Büll L. T., Guppy C. N., Santos S. de M. C. and Moreira L. L. Q. (2020) Effects of lime and steel slag application on soil fertility and soybean yield under a no till-system. *Soil Tillage Res.* **196**, 104422.

Evans E. H. and Clough R. (2005) ISOTOPE DILUTION ANALYSIS. In *Encyclopedia of Analytical Science (Second Edition)* (eds. P. Worsfold, A. Townshend, and C. Poole). Elsevier, Oxford. pp. 545–553.

Gillman G. P., Burkett D. C. and Coventry R. J. (2001) A laboratory study of application of basalt dust to highly weathered soils: effect on soil cation chemistry. *Soil Res.* **39**, 799–811.

Gillman G. P., Burkett D. C. and Coventry R. J. (2002) Amending highly weathered soils with finely ground basalt rock. *Appl. Geochem.* **17**, 987–1001.

Guo F., Wang Y., Zhu H., Zhang C., Sun H., Fang Z., Yang J., Zhang L., Mu Y., Man Y. B. and Wu F. (2023) Crop productivity and soil inorganic carbon change mediated by enhanced rock weathering in farmland: A comparative field analysis of multi-agroclimatic regions in central China. *Agric. Syst.* **210**, 103691.

Haque F., Santos R. M. and Chiang Y. W. (2020) Optimizing Inorganic Carbon Sequestration and Crop Yield With Wollastonite Soil Amendment in a Microplot Study. *Front. Plant Sci.* **11**.

IEA (2022) *Carbon Capture, Utilization, and Storage*., International Energy Agency Paris.

IPCC (2018) *Global Warming of 1.5 °C.*,

Jariwala H., Haque F., Vanderburgt S., Santos R. M. and Chiang Y. W. (2022) Mineral–Soil–Plant–Nutrient Synergisms of Enhanced Weathering for Agriculture: Short-Term Investigations Using Fast-Weathering Wollastonite Skarn. *Front. Plant Sci.* **13**.

Kantola I. B., Blanc-Betes E., Masters M. D., Chang E., Marklein A., Moore C. E., von Haden A., Bernacchi C. J., Wolf A., Epihov D. Z., Beerling D. J. and DeLucia E. H. (2023) Improved net carbon budgets in the US Midwest through direct measured impacts of enhanced weathering. *Glob. Change Biol.* **n/a**.

Kelemen P., Benson S. M., Pilorgé H., Psarras P. and Wilcox J. (2019) An Overview of the Status and Challenges of CO2 Storage in Minerals and Geological Formations. *Front. Clim.* **1**.

Knapp W. J., Stevenson E. I., Renforth P., Ascough P. L., Knight A. C. G., Bridgestock L., Bickle M. J., Lin Y., Riley A. L., Mayes W. M. and Tipper E. T. (2023) Quantifying CO2 Removal at Enhanced Weathering Sites: a Multiproxy Approach. *Environ. Sci. Technol.* **57**, 9854–9864.

Nadeem S., Bakken L. R., Frostegård Å., Gaby J. C. and Dörsch P. (2020) Contingent Effects of Liming on N2O-

Emissions Driven by Autotrophic Nitrification. *Front. Environ. Sci.* **8**.

National Academies of Sciences Engineering and Medicine (2019) *Negative Emissions Technologies and Reliable Sequestration: A Research Agenda*., The National Academies Press, Washington, DC.

Piatak N. M., Parsons M. B. and Seal II R. R. (2015) Characteristics and environmental aspects of slag: a review. *Appl. Geochem.* **57**, 236–266.

Puro.earth (2022) Enhanced Rock Weathering Methodology.

Reershemius T., Kelland M. E., Jordan J. S., Davis I. R., D'Ascanio R., Kalderon-Asael B., Asael D., Suhrhoff T. J., Epihov D. Z., Beerling D. J., Reinhard C. T. and Planavsky N. J. (2023) Initial Validation of a Soil-Based Mass-Balance Approach for Empirical Monitoring of Enhanced Rock Weathering Rates. *Environ. Sci. Technol.* **57**, 19497–19507.

Renforth P., Washbourne C.-L., Taylder J. and Manning D. A. C. (2011) Silicate Production and Availability for Mineral Carbonation. *Environ. Sci. Technol.* **45**, 2035–2041.

Riebe C. S., Kirchner J. W. and Finkel R. C. (2003) Long-term rates of chemical weathering and physical erosion from cosmogenic nuclides and geochemical mass balance. *Geochim. Cosmochim. Acta* **67**, 4411–4427.

Sikora F. J. (2006) A Buffer that Mimics the SMP Buffer for Determining Lime Requirement of Soil. *Soil Sci. Soc. Am. J.* **70**, 474–486.

Smith S., Geden O., Nemet G., Gidden M., Lamb W., Powis C., Bellamy R., Callahan M., Cowie A., Cox E., Fuss S., Gasser T., Grassi G., Greene J., Lueck S., Mohan A., Müller-Hansen F., Peters G., Pratama Y. and Minx J. (2023) *The State of Carbon Dioxide Removal - 1st Edition*.,

Stracke A., Scherer E. E. and Reynolds B. C. (2014) 15.4 - Application of Isotope Dilution in Geochemistry. In *Treatise on Geochemistry (Second Edition)* (eds. H. D. Holland and K. K. Turekian). Elsevier, Oxford. pp. 71–86.

Strefler J., Amann T., Bauer N., Kriegler E. and Hartmann J. (2018) Potential and costs of carbon dioxide removal by enhanced weathering of rocks. *Environ. Res. Lett.* **13**, 034010.

Tilley D. B. and Eggleton R. A. (2005) Titanite Low-Temperature Alteration and Ti Mobility. *Clays Clay Miner.* **53**, 100–107.

UNEP (2017) *The Emissions Gap Report 2017*., United Nations Environment Programme (UNEP), Nairobi.

UNFCCC (2015) *Paris Agreement to the United Nations Framework Convention on Climate Change*.,

USDA (2022) *Farms and Land in Farms: 2021 Summary*., United States Department of Agriculture.

USGS (2015) Map of Worldwide Croplands.

Vibbert H. B. and Park A.-H. A. (2022) Harvesting, storing, and converting carbon from the ocean to create a new carbon economy: Challenges and opportunities. *Front. Energy Res.* **10**.

White Art F. (1995) Chemical Weathering Rates of Silicate Minerals. In (eds. Arthur F. White and S. L. Brantley). De Gruyter. pp. 407–462.

APPENDIX

Table 1: Mineralogical composition, in weight percent, of basalt feedstock used in EMW trial plots at Carleton College, Northfield, Minnesota. Data was collected via powder X-Ray Diffraction (XRD).

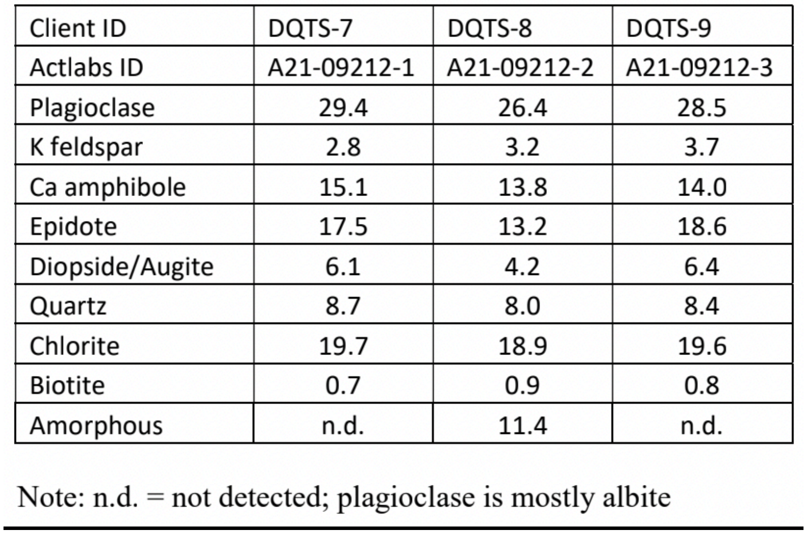

Client ID	DQTS-7	DQTS-8	DQTS-9
Actlabs ID	A21-09212-1	A21-09212-2	A21-09212-3
Plagioclase	29.4	26.4	28.5
K feldspar	2.8	3.2	3.7
Ca amphibole	15.1	13.8	14.0
Epidote	17.5	13.2	18.6
Diopside/Augite	6.1	4.2	6.4
Quartz	8.7	8.0	8.4
Chlorite	19.7	18.9	19.6
Biotite	0.7	0.9	0.8
Amorphous	n.d.	11.4	n.d.

Note: n.d. = not detected; plagioclase is mostly albite

Table 2: Mineralogical composition, in weight percent, of steel slag feedstock acquired from Plant Tuff Inc. used in EMW trial plots at Carleton College, Northfield, Minnesota. Data was collected via powder X-Ray Diffraction (XRD).

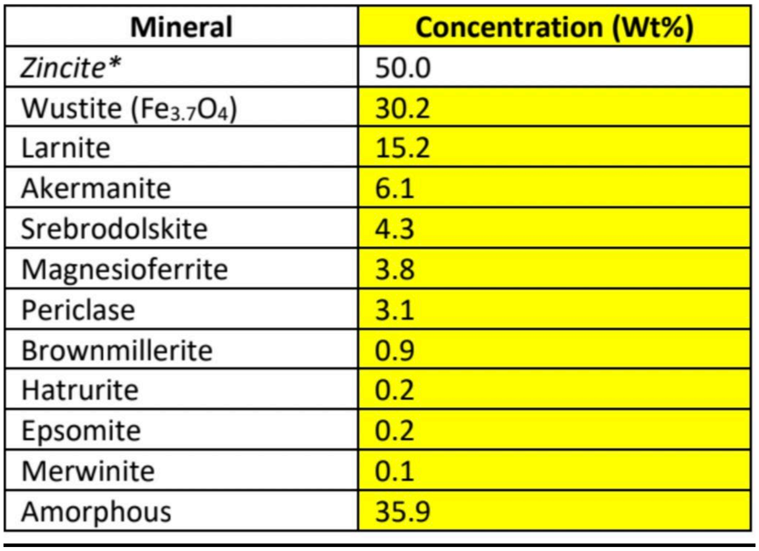

Mineral	Concentration (Wt%)
*Zincite**	50.0
Wustite ($Fe_{3.7}O_4$)	30.2
Larnite	15.2
Akermanite	6.1
Srebrodolskite	4.3
Magnesioferrite	3.8
Periclase	3.1
Brownmillerite	0.9
Hatrurite	0.2
Epsomite	0.2
Merwinite	0.1
Amorphous	35.9

Table 3: Baseline, expected, and measured elemental concentrations and percentage differences from EMW trial plots at Carleton College, Northfield, Minnesota.

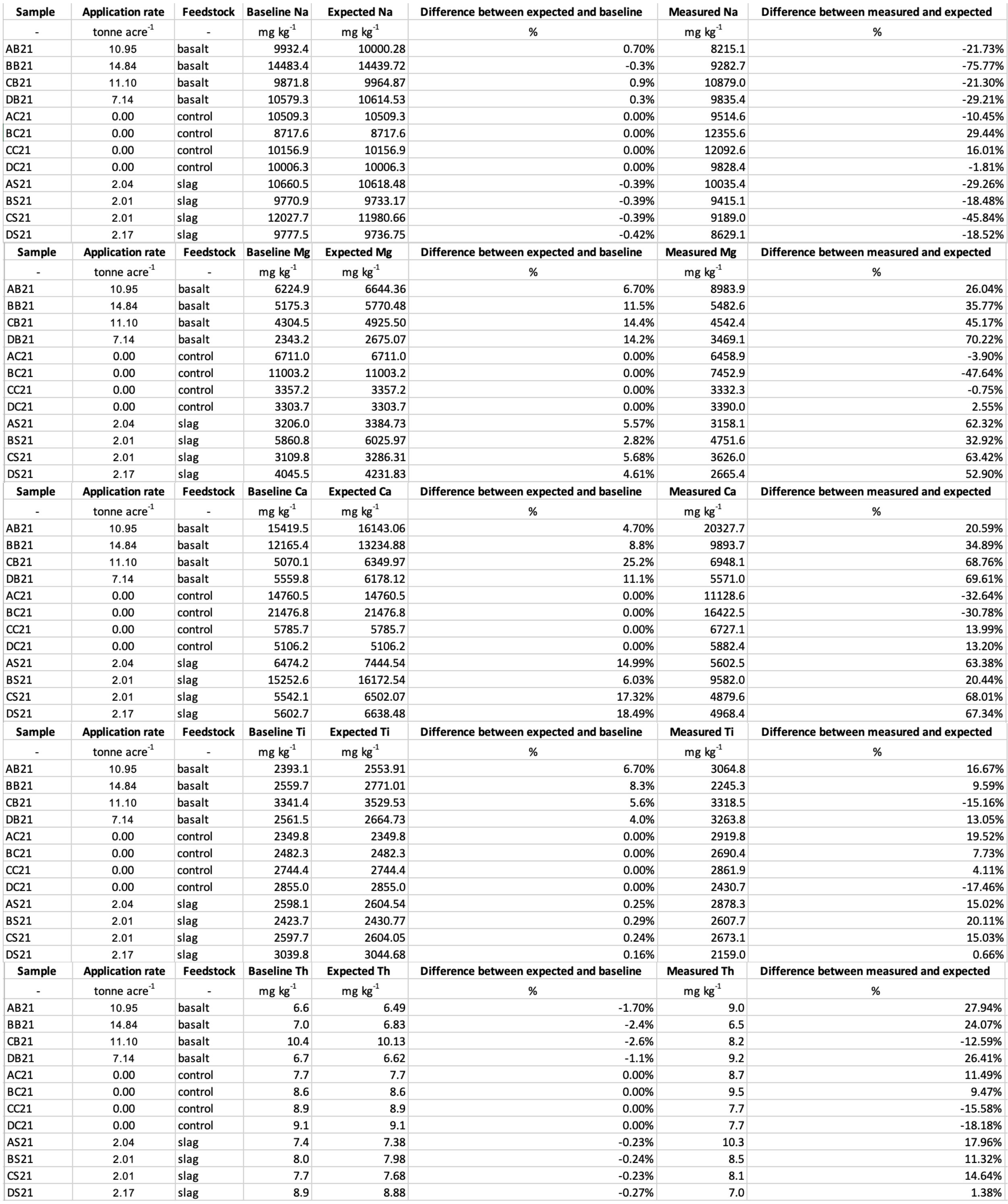

Sample	Application rate	Feedstock	Baseline Na	Expected Na	Difference between expected and baseline	Measured Na	Difference between measured and expected
-	tonne acre^{-1}	-	mg kg^{-1}	mg kg^{-1}	%	mg kg^{-1}	%
AB21	10.95	basalt	9932.4	10000.28	0.70%	8215.1	-21.73%
BB21	14.84	basalt	14483.4	14439.72	-0.3%	9282.7	-75.77%
CB21	11.10	basalt	9871.8	9964.87	0.9%	10879.0	-21.30%
DB21	7.14	basalt	10579.3	10614.53	0.3%	9835.4	-29.21%
AC21	0.00	control	10509.3	10509.3	0.00%	9514.6	-10.45%
BC21	0.00	control	8717.6	8717.6	0.00%	12355.6	29.44%
CC21	0.00	control	10156.9	10156.9	0.00%	12092.6	16.01%
DC21	0.00	control	10006.3	10006.3	0.00%	9828.4	-1.81%
AS21	2.04	slag	10660.5	10618.48	-0.39%	10035.4	-29.26%
BS21	2.01	slag	9770.9	9733.17	-0.39%	9415.1	-18.48%
CS21	2.01	slag	12027.7	11980.66	-0.39%	9189.0	-45.84%
DS21	2.17	slag	9777.5	9736.75	-0.42%	8629.1	-18.52%
Sample	Application rate	Feedstock	Baseline Mg	Expected Mg	Difference between expected and baseline	Measured Mg	Difference between measured and expected
-	tonne acre^{-1}	-	mg kg^{-1}	mg kg^{-1}	%	mg kg^{-1}	%
AB21	10.95	basalt	6224.9	6644.36	6.70%	8983.9	26.04%
BB21	14.84	basalt	5175.3	5770.48	11.5%	5482.6	35.77%
CB21	11.10	basalt	4304.5	4925.50	14.4%	4542.4	45.17%
DB21	7.14	basalt	2343.2	2675.07	14.2%	3469.1	70.22%
AC21	0.00	control	6711.0	6711.0	0.00%	6458.9	-3.90%
BC21	0.00	control	11003.2	11003.2	0.00%	7452.9	-47.64%
CC21	0.00	control	3357.2	3357.2	0.00%	3332.3	-0.75%
DC21	0.00	control	3303.7	3303.7	0.00%	3390.0	2.55%
AS21	2.04	slag	3206.0	3384.73	5.57%	3158.1	62.32%
BS21	2.01	slag	5860.8	6025.97	2.82%	4751.6	32.92%
CS21	2.01	slag	3109.8	3286.31	5.68%	3626.0	63.42%
DS21	2.17	slag	4045.5	4231.83	4.61%	2665.4	52.90%
Sample	Application rate	Feedstock	Baseline Ca	Expected Ca	Difference between expected and baseline	Measured Ca	Difference between measured and expected
-	tonne acre^{-1}	-	mg kg^{-1}	mg kg^{-1}	%	mg kg^{-1}	%
AB21	10.95	basalt	15419.5	16143.06	4.70%	20327.7	20.59%
BB21	14.84	basalt	12165.4	13234.88	8.8%	9893.7	34.89%
CB21	11.10	basalt	5070.1	6349.97	25.2%	6948.1	68.76%
DB21	7.14	basalt	5559.8	6178.12	11.1%	5571.0	69.61%
AC21	0.00	control	14760.5	14760.5	0.00%	11128.6	-32.64%
BC21	0.00	control	21476.8	21476.8	0.00%	16422.5	-30.78%
CC21	0.00	control	5785.7	5785.7	0.00%	6727.1	13.99%
DC21	0.00	control	5106.2	5106.2	0.00%	5882.4	13.20%
AS21	2.04	slag	6474.2	7444.54	14.99%	5602.5	63.38%
BS21	2.01	slag	15252.6	16172.54	6.03%	9582.0	20.44%
CS21	2.01	slag	5542.1	6502.07	17.32%	4879.6	68.01%
DS21	2.17	slag	5602.7	6638.48	18.49%	4968.4	67.34%
Sample	Application rate	Feedstock	Baseline Ti	Expected Ti	Difference between expected and baseline	Measured Ti	Difference between measured and expected
-	tonne acre^{-1}	-	mg kg^{-1}	mg kg^{-1}	%	mg kg^{-1}	%
AB21	10.95	basalt	2393.1	2553.91	6.70%	3064.8	16.67%
BB21	14.84	basalt	2559.7	2771.01	8.3%	2245.3	9.59%
CB21	11.10	basalt	3341.4	3529.53	5.6%	3318.5	-15.16%
DB21	7.14	basalt	2561.5	2664.73	4.0%	3263.8	13.05%
AC21	0.00	control	2349.8	2349.8	0.00%	2919.8	19.52%
BC21	0.00	control	2482.3	2482.3	0.00%	2690.4	7.73%
CC21	0.00	control	2744.4	2744.4	0.00%	2861.9	4.11%
DC21	0.00	control	2855.0	2855.0	0.00%	2430.7	-17.46%
AS21	2.04	slag	2598.1	2604.54	0.25%	2878.3	15.02%
BS21	2.01	slag	2423.7	2430.77	0.29%	2607.7	20.11%
CS21	2.01	slag	2597.7	2604.05	0.24%	2673.1	15.03%
DS21	2.17	slag	3039.8	3044.68	0.16%	2159.0	0.66%
Sample	Application rate	Feedstock	Baseline Th	Expected Th	Difference between expected and baseline	Measured Th	Difference between measured and expected
-	tonne acre^{-1}	-	mg kg^{-1}	mg kg^{-1}	%	mg kg^{-1}	%
AB21	10.95	basalt	6.6	6.49	-1.70%	9.0	27.94%
BB21	14.84	basalt	7.0	6.83	-2.4%	6.5	24.07%
CB21	11.10	basalt	10.4	10.13	-2.6%	8.2	-12.59%
DB21	7.14	basalt	6.7	6.62	-1.1%	9.2	26.41%
AC21	0.00	control	7.7	7.7	0.00%	8.7	11.49%
BC21	0.00	control	8.6	8.6	0.00%	9.5	9.47%
CC21	0.00	control	8.9	8.9	0.00%	7.7	-15.58%
DC21	0.00	control	9.1	9.1	0.00%	7.7	-18.18%
AS21	2.04	slag	7.4	7.38	-0.23%	10.3	17.96%
BS21	2.01	slag	8.0	7.98	-0.24%	8.5	11.32%
CS21	2.01	slag	7.7	7.68	-0.23%	8.1	14.64%
DS21	2.17	slag	8.9	8.88	-0.27%	7.0	1.38%